Applied Energy 199 (2017) 180–186

Contents lists available at ScienceDirect

Applied Energy

journal homepage: www.elsevier.com/locate/apenergy

Durable direct ethanol anode-supported solid oxide fuel cell

M.C. Steil [a,b], S.D. Nobrega [a,b,c], S. Georges [a,b], P. Gelin [d], S. Uhlenbruck [e], F.C. Fonseca [c,*]

[a] Université Grenoble Alpes, LEPMI, F-38000 Grenoble, France
[b] CNRS, LEPMI, F-38000 Grenoble, France
[c] Univ Lyon, Université Claude Bernard Lyon 1, CNRS, IRCELYON, F-69626 Villeurbanne, France
[d] Forschungszentrum Jülich GmbH, Institute of Energy and Climate Research, Materials Synthesis and Processing (IEK-1), 52425 Jülich, Germany
[e] Instituto de Pesquisas Energéticas e Nucleares, IPEN-CNEN/SP, 05508-000 São Paulo, SP, Brazil

HIGHLIGHTS

- Direct ethanol anode-supported SOFC stable for 600 h without water.
- High-performance SOFC exhibiting similar current output in both hydrogen and ethanol.
- Ceria-based catalytic layer ensures ethanol conversion and avoids carbon deposits.

ARTICLE INFO

Article history:
Received 11 January 2017
Received in revised form 27 March 2017
Accepted 28 April 2017
Available online 9 May 2017

Keywords:
Direct alcohol solid oxide fuel cell
Bioethanol
Catalytic layer
Ceria-based catalyst

ABSTRACT

Anode-supported solid oxide fuel cells accumulating more than 700 h of stable operation on dry ethanol with high current output are reported. A highly active ceria-based catalytic layer deposited onto the anode efficiently converts the primary fuel into hydrogen using the electrochemically generated steam. On the other hand, standard fuel cells without the catalytic layer collapse because of carbon deposit formation within the initial 5 h of operation with ethanol. The nanostructured ceria-based catalyst forms a continuous porous layer (~25 μm thick) over the Ni-based anode support that has no apparent influence on the fuel cell operation and prevents carbon deposit formation. Moreover, the catalytic layer promotes overall steam reforming reactions of ethanol that result in similar current outputs in both hydrogen and ethanol fuels. The stability of single cells, with relatively large active area (8 cm^2), confirms the feasibility of a catalytic layer for internal reforming of biofuels in solid oxide fuel cells. The experimental results provide a significant step towards the practical application of direct ethanol solid oxide fuel cells.

1. Introduction

The greenhouse gas emissions resulting from the combustion of fossil fuel have been directly related to the measured temperature rise around the planet. In this scenario, the historical combination of oil-derived fuels and combustion engines requires urgent alternatives to meet the 2 °C global warming limit recently defined [1]. The development of more efficient and environmentally friendly energy sources has gained vital importance to avoid a legacy of irreversible environmental damage for future generations. In this context, fuel cells and the so-called hydrogen economy have attracted a great deal of attention as a promising evolution of energy systems to contribute for more efficient and clean energy production. Fuel cells are electrochemical converters not limited to the Carnot cycle, with theoretical efficiency exceeding 80%, and water as the only residue released to the atmosphere when hydrogen is used. Among fuel cells, solid oxide fuel cells (SOFCs) are potentially the most efficient technology to convert chemical energy into electricity and thus could have a major impact on reducing fuel consumption and CO_2 emissions [2–5]. However, a critical issue is that hydrogen must be produced from other primary sources. Most of hydrogen is obtained from steam reforming of natural gas, requiring additional carbon capture technologies to ensure a complete carbon neutral cycle. Methane is the most studied alternative fuel for SOFCs due to availability and possible internal reforming [4,6–11].

Considerably less attention has been given to the use of renewable fuels in SOFCs, though the direct use of SOFCs with biofuels has been proposed as the most energy efficient means to use homegrown carbon neutral fuels [5,12–14]. Among available biofuels the most produced worldwide and probably the most advanced one is ethanol with notable application in transportation [14–16]. Bioethanol is efficiently produced from renewable bio-

* Corresponding author.
E-mail address: fabiocf@usp.br (F.C. Fonseca).

http://dx.doi.org/10.1016/j.apenergy.2017.04.086
0306-2619/

mass and is an economically viable energy source for large-scale production, generating low emissions and bringing positive impact to the economy and the environment [14–16]. Nonetheless, as compared to methane, a limited number of studies is dedicated to ethanol SOFCs [17–20]. More recently, such a renewable and available liquid biofuel has gained increasing attention as a promising SOFC fuel, as reported in several studies [15–24]. Liquid fuels compensate the need of engineering optimization for fuel delivery with easier storage, handling and transportation than gas fuels. Such a trend has been confirmed by the announcement of an ethanol SOFC prototype vehicle by Nissan, expected to be commercialized in 2020 [25]. The e-bio fuel cell concept is the first to use ethanol for electric power generation with an SOFC for vehicular application. This carbon neutral vehicle brings together the advantages of a liquid and renewable biofuel to power electric cars and it is a perfect example of the applicability of ethanol SOFCs. It is interesting to notice that Nissan's prototype uses a pre-reformer, whereas our study aims at improving the technology to (direct) internal reforming of bioethanol.

The high operating temperatures of SOFCs allow the direct conversion of primary fuels (e.g., natural gas and ethanol) into electricity [2–11]. However, the stable operation of SOFCs running on fuels containing carbon is still a challenge because Ni, from the standard anode yttria-stabilized zirconia (YSZ)-Ni cermet, promotes the dehydrogenation of fuel. Such reactions result in carbon deposition on the surface of the anode, causing an irreversible degradation that has hampered a more widespread use of SOFCs [4–6]. Two main strategies have been developed to allow the use of such fuels in SOFC. The first one is the addition of an oxidizing agent to the fuel stream to prevent the thermodynamic conditions that favor carbon deposition [4,25]. Usually, water is the most common choice, but some studies have reported SOFCs running on methane by adding air or CO_2 [26]. Nonetheless, the addition of large amounts of water (or air) in the fuel stream reduces the overall efficiency and adds complexity to the system. The second strategy is to modify or substitute the traditional Ni-based cermet anode to allow stable operation of SOFCs without fuel dilution. Different materials have been reported, including various cermets and ceramic anodes [4,10,27]. However, such anodes usually exhibit either low electronic conductivity or low catalytic activity [4,6,10]. Finding a material (single phase or composite) that combines high catalytic activity and high conductivity along with other SOFC requirements (stability, compatibility, cost, etc.) is a hard task. Indeed, no alternative anode has shown performance equivalent to that of the standard Ni-YSZ running on hydrogen [4,10]. Therefore, preserving the Ni cermet and adding a catalyst tailored for a desired fuel is a promising strategy for SOFC anode design [12,13,19,20].

In this context, using a bi-layer anode has the advantage of using the best-known anode (Ni-YSZ) for hydrogen along with a suitable catalyst. Latest generation of SOFCs is a multilayer device in which several elaborated functional layers were incorporated to the initial anode/electrolyte/cathode arrangement. Two marked examples of layers incorporated to SOFC to enhance both performance and durability are: (i) gadolinia-doped ceria (CGO) diffusion barrier to avoid undesired reactions between the cobalt-iron lanthanum perovskite (LSCF) cathodes and YSZ electrolyte; and (ii) Cr-poisoning has been reduced by coating metallic interconnectors with spinels. Therefore, it's reasonable that a similar strategy is being used on the anode side to allow the operation of SOFCs on alternative fuels [12,13].

In general, direct ethanol SOFC tests revealed that switching fuel from H_2 to ethanol decreases the overall performance of the fuel cell and most of the reported results use some additional oxidant agent (usually water) [16,19–21]. More importantly, studies demonstrating long-term stability tests on ethanol are seldom reported. Thus, in the present study, to ensure the stability of the studied fuel cells we have investigated the SOFC operation on ethanol in harsh dry conditions (without adding water), inspired by the gradual internal reforming (GIR) [4,28]. The main idea of GIR is that the fuel is progressively reformed along the anode (the reactor) with only an initial addition of a small amount of water [4]. Such small amount of water is needed at the fuel inlet of the anode (reactor) to initiate the reforming activity [4,28]. Water plays partly the role of controlling the activity, making both catalytic and electrochemical functions intimately mixed together. Conceptually differently, the results here presented were obtained by separating catalytic and electrochemical reactions in two different layers of the anode [29–32].

The reactions of the direct ethanol single cell with catalytic layer are depicted in Fig. 1.

The role of the catalytic layer is to convert most of the fuel into H_2 and CO_2 by steam reforming before reaching the Ni-YSZ anode, thus preventing carbon deposition at the cermet. The catalytic reaction needs water to proceed. Water is provided by the electrochemical reactions at the cermet while the catalytic reforming reaction provides H_2 for the cermet. The global reaction for ethanol steam reforming results in six molecules of hydrogen, which are ideally converted to 12 electrons by the electrochemical oxidation of H_2 reaction at the anode/electrolyte interface. Thus, dry ethanol theoretically results in a number of electrons six times higher than that of the reaction of pure hydrogen. Moreover, water produced in the anode is in excess for the stoichiometric steam reforming. This operating procedure was previously demonstrated for electrolyte-supported button cells running with dry fuels such as methane and ethanol [22,29,31]. The catalytic layer was composed of $Ce_{0.9}Gd_{0.1}O_{2-x}$ promoted with Ir in trace amounts (Ir-CGO). This catalyst was shown to be active in both methane and ethanol reforming while being highly resistant to carbon deposition in water deficient conditions (conditions thermodynamically favorable to carbon formation). Two main aspects were investigated in previous reports: the catalytic activity for fuel conversion in SOFCs, and short-term stability [22,29–32]. Nonetheless, fuel cell performance in such previous studies was limited by a relatively low current output due to thick electrolyte supports [22,29–32]. As compared to electrolyte-supported cells, the anode-supported ones exhibit both higher Ni content and higher reaction rates that could favor carbon deposition. Additionally, mass transport of reactants and reaction products through the electrode must be preserved when the active layer is added to the anode support. Such features are potentially detrimental for the performance of anode-supported SOFCs with a catalytic layer. Therefore, validating the concept of a bilayer anode in high-performance direct-ethanol SOFC is paramount for

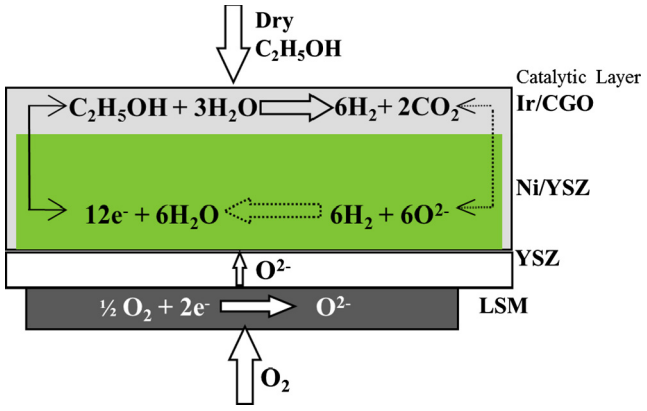

Fig. 1. Schematics of the anode supported cell (not in scale) and the theoretical reactions taking place in each component.

advancing such devices towards practical application. Thus, in the present study we demonstrate that high-performance anode supported fuel cells can use a catalytic layer to run on a renewable liquid biofuel, with high stability and delivering practically the same current output as in hydrogen.

2. Experimental

Anode-supported single cells using 8 mol% yttria-stabilized zirconia - YSZ (~10 μm thickness), $La_{0.65}Sr_{0.30}MnO_3$ -based cathode (32 mm diameter, 8 cm^2 active area), and Ni-YSZ (42 mm diameter and ~600 μm thickness) anode were fabricated at Forschungszentrum Jülich (FZJ, Germany) [33].

A gadolinia-doped ceria ($Ce_{0.9}Gd_{0.1}O_{2-x}$, CGO) containing 0.1 wt.% of Ir catalyst was prepared by incipient wetness impregnation technique, using CGO (Praxair, 43 m^2g^{-1}) and iridium acethylacetonate (Aldrich) in toluene. Solvent was removed under reduced pressure and catalyst calcined at 350 °C for 6 h, as described in detail elsewhere [34]. Catalyst characterization was carried out by transmission electron microscopy (TEM, Titan FEI ETEM 80-300KeV G2) and specific surface area measurements (Micromeritics, ASAP 2020). Such analyses were performed on both the as-prepared and Ir-CGO powders thermally treated at 900 °C for 2 h under Ar (1 ppm O_2). The catalytic ink was prepared by mixing the following components (wt.%): 40% (80 vol.% Ir-CGO +20 vol.% cellulose, SigmaCell – 20 μm), 30% ethanol, 27% terpineol, 2% PVB, and 1% PVP. Mixing of the ink components was carried out for 12 h in a turbula mixer (WAB). The ink was deposited onto the anode by using an air spray valve (SV 600) with a controller (VM60, Eleco EFD) mounted on a table tabletop robot (TTA, IAI Corp.). After ink deposition, the sample was heat treated in air at 500 °C for 2 h to promote removal of organics, and at 900 °C for 2 h under Ar to ensure adhesion of the catalytic layer. The total amount of the catalyst deposited in a single cell was ~0.2 g. Scanning electron microscopy (SEM) images were collected to analyze the microstructure of the deposited catalytic layer.

For the electrochemical performance tests, current collectors were attached to the single cell. On the anode side, the gold current collector was prepared before the deposition of the catalytic layer. A gold ink was used both to paint a gold mesh (~0.12 cm^2) over the surface of the anode and to fix a gold wire, connected to the mesh, along the perimeter of the support; followed by curing at 900 °C in air. Two extensions of the gold wire coming out of the anode surface were left uncovered by the ceria layer to ensure good electrical contact. On the cathode side, current collector was a platinum mesh mechanically connected to the electrode. The anode-supported cells were tested in a house-made rig at 850 °C with flowing air (8 L h^{-1}) in the cathode side [22,31,35]. Fuel cells were initially operated on H_2 (60%), balanced with Ar (40%), with total fuel flow rates between 4 and 12 L h^{-1} [35]. The fuel residence time in the fuel cell test setup is ~20 s. After anode reduction (following the protocol used at FZJ) and stable OCV ~1.1 V obtained at measuring temperature (850 °C), the electrochemical properties were characterized firstly under hydrogen [35]. In this operation mode, two successive steps are required for the SOFC system to be started properly. Firstly, the cell has to be operated in pure H_2 in order to produce some amount of water, which slowly diffuses through the catalytic layer. In a second step, H_2 can be substituted by the dry fuel (hydrocarbon or alcohol), which is converted into H_2 by reacting with water present in the catalytic layer. Once initiated both catalytic and electrochemical reactions sustain each other [29–32]. Thus, hydrogen was progressively switched to (dry) ethanol. Ideally, steam reforming of 1 mol of ethanol produces 6 mol of H_2 (Fig. 1). It is important to point out that fuel concentration during testing was carefully controlled in order to keep the theoretical number of electrons constant when hydrogen (60%) is changed to ethanol (10%) with the same total flow rate [23,31,35]. Such a control is rarely taken into account in reported studies when H_2 is substituted for an alternative fuel.

Ethanol was kept in a thermal bath with a controlled temperature (29 °C) and carried by Ar with same total flow rate as H_2. Current vs. time (i - t) measurements, at constant cell polarization (V = 0.6 or 0.7 V), were performed by an Autolab PGSTAT128N potentiostat with a BSTR10A current booster.

Durability tests of continuous operation under ethanol at constant polarization of the anode-supported cells were performed with maximum duration of 25 days. Post-test analyses of fuel cells included energy-dispersive X-ray (EDS) and SEM experiments on fractured surfaces of the anode to investigate possible carbon deposition. The carbon content of tested samples was measured using a Leco CS600 analyzer. The entire cell was heated in an oxygen stream, and the resulting amount of CO/CO_2 was determined by infrared spectroscopy.

As a comparison of a standard fuel cell running on ethanol, an electrolyte-supported fuel cell with same components, but without catalytic layer, was fabricated as described elsewhere [22,31]. Electrolyte support thickness was 500 μm and final thickness of anode and cathode was 60 and 70 μm, respectively, with 13.8 cm^2 active area. This fuel cell configuration has a much lower Ni loading and it is less prone to coke formation, as compared to the anode supported cell. Fuel cell testing was performed in the same rig under similar conditions [22,31]. The fuel cell was tested at 850 °C with (dry) ethanol (14%) carried by Ar at flow rates in the 4–12 L h^{-1} range. The performance of the standard electrolyte-supported fuel cell was evaluated by sequentially measuring i - V curves at 30 min. intervals during total operation time of 5 h.

3. Results and discussion

Direct ethanol testing on electrolyte-supported fuel cells without catalytic layer are shown in Fig. 2. It is generally accepted that the standard cermet anode will collapse because carbon deposits over Ni when hydrocarbon or alcohol fuels are directly fed to the SOFC [36]. However, few reports have shown the time dependence of such degradation. After anode reduction and initial operation on hydrogen, fuel was switched to (dry) ethanol. The OCV dropped from ~1.15 V in H_2 to ~0.95 V in ethanol, and a performance decay is observed over the entire i range of the polarization curve. The fuel cell ran with good stability during initial ~3 h, as inferred from comparable i - V data taken in this time interval. However, further increasing operating time under ethanol resulted in a rapid performance degradation that caused fuel cell collapse after ~4.5 h. A

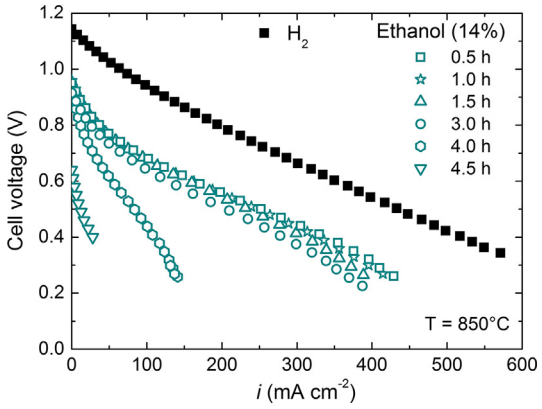

Fig. 2. Polarization curves on hydrogen and dry ethanol for standard electrolyte-supported SOFC without catalytic layer.

large amount of carbon deposits was evident all over the sample and measuring apparatus after testing. Such results indicate that long-term stability tests are crucial for evaluating fuel cells running on ethanol and, more importantly, that a functional anode is required to ensure durable direct ethanol SOFCs.

Gas phase reaction is a first issue when using alternative fuels in SOFCs. As indicated in Fig. 1, the stoichiometric reaction of the catalytic steam reforming (SR) of ethanol [37] is:

$$C_2H_5OH + 3H_2O \rightarrow 6H_2 + 2CO_2 \quad (1)$$

However, many other reactions can occur simultaneously with hydrogen production reactions [37]. Ethanol may be dehydrogenated to acetaldehyde or dehydrated to ethylene. Thus, ethanol decomposes at high temperature and depending on fuel cell operating parameters (temperature, fuel utilization, flow rate, current output, etc.) an accurate determination of present species can be a hard task [38,39],. At 850 °C, homogenous decomposition of ethanol was found to result in water along with H_2 (34%), CO (28%), CH_4 (23%), and ethylene (15%), according to previous experiments [22]. Except for ethylene, the resulting products correspond to a fuel gas mixture for SOFCs. However, ethylene, resulting from ethanol dehydration, is a known source for carbon deposits and must be totally converted for stable operation of the fuel cell [39]. Such a feature is particularly important for the SOFC test rig, which has fuel residence time one order of magnitude higher than that of typical systems used for catalytic tests (~1 s).

Thus, a direct ethanol SOFC requires, basically, anodes active towards CH_4 and C_2H_4 conversion. Indeed, CH_4 and C_2H_4 are the two undesired products resulting from steam reforming or homogeneous pyrolysis of ethanol. Interestingly, in the presence of Ir-CGO, ethanol was shown to be converted into H_2, CO and CO_2, while C_2H_4 could not be detected and CH_4 formed in very low amount [22]. The Ir addition to CGO enhances the ethanol dehydrogenation rate, as usually observed over noble metals catalysts, and promotes the steam reforming of methane thus produced [29,34,40],. Moreover, this catalyst was shown to prevent the formation of carbon deposits [40]. This demonstrated that Ir-CGO is a suitable catalyst for this application [22,29,34,40],. Fig. 3 shows images of the catalyst (TEM) and the catalytic layer (FEG-SEM) after heat treatment at 900 °C under Ar. In Fig. 3a TEM image shows that catalyst displays some agglomeration after the heat treatment, but still individual particles can be discerned. Gadolinia-doped ceria faceted nanoparticles with rectangular shape and typical dimensions of ~40 nm are observed. Iridium nanoparticles can be identified as isolated dark dots segregated at the surface of CGO particles with an average diameter ~4 nm. Recently, high-resolution TEM experiments have shown a very fine and homogenous dispersion of small and isolated Ir particles over CGO substrates [41]. Iridium particles have sizes ranging from 2 to 6 nm and are very resistant towards coalescence, as inferred from TEM images taken before and after catalyst tests [41].

The specific surface area of the as-prepared catalyst was close to that of CGO (45 $m^2 g^{-1}$); however, treating the catalyst powders in the same conditions used for sintering the catalytic layers (900 °C in 1 ppm O_2) results in a decrease of specific surface area to 10 $m^2 g^{-1}$. The CGO precursor is a highly active powder that may exhibit particle coarsening, or even sintering, at relatively low temperatures. Thus, in order to use this material as a catalytic layer a compromise between adhesion to the anode and high surface area for catalytic reactions must be observed. Moreover, the catalytic layer should have no interference on the mass transport of the fuel cell, i.e., the catalytic layer should combine thickness and porosity compatible with the anode support to avoid additional impedance for gas flow. The SEM images in Fig. 3b and c show the cross section at the interface between anode support and the sintered catalytic layer. The active layer has ~25 μm thickness and continuously

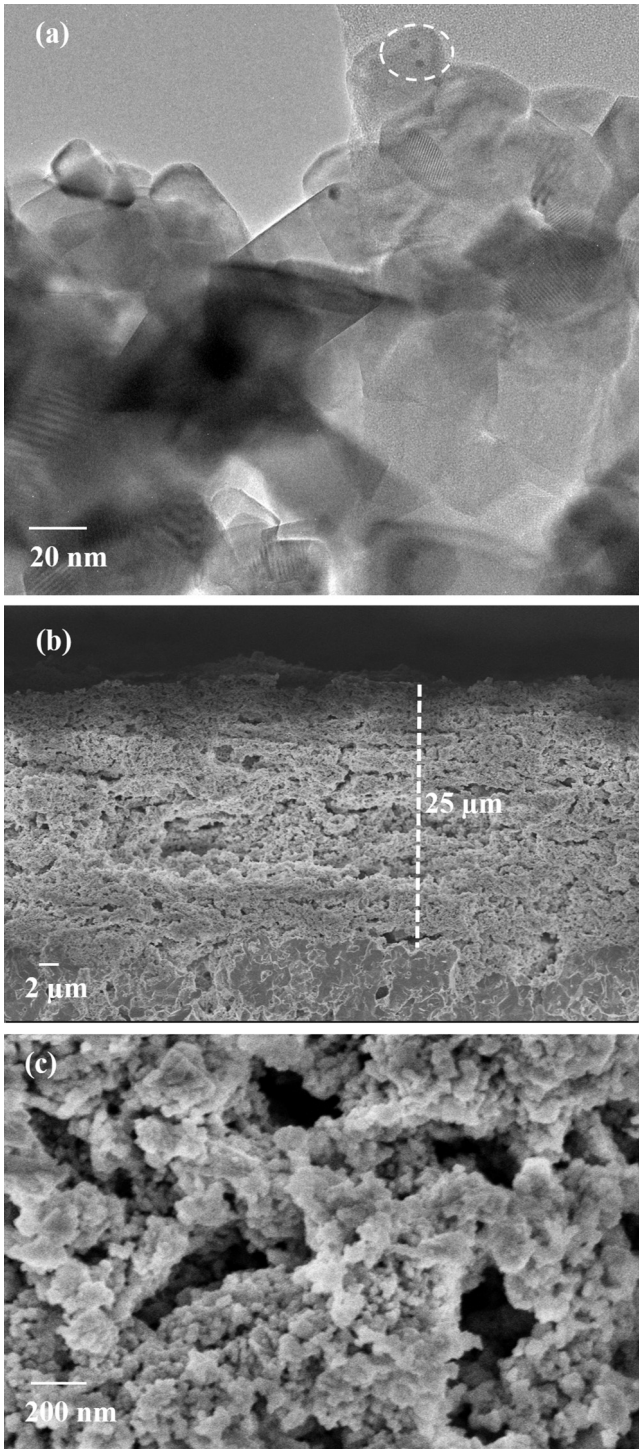

Fig. 3. (a) TEM image of the Ir-CGO catalyst after heat treatment at 900 °C in Ar (iridium nanoparticles are marked by the dotted circle); (b) SEM image of the interface between anode support and catalytic layer; (c) higher magnification SEM image of the catalytic layer.

coats the anode outer surface with a good adhesion. Solid state reaction between YSZ and CGO is usually observed at temperatures above 1100 °C in air [42,43],. Indeed, the interface between the current-collector anode and the catalyst exhibits no sign of undesired reaction. The catalytic layer coated the outer surface of the anode; however, it is possible to observe that the Ir-CGO has higher porosity than the anode (before reduction). The heat treatment at 900 °C in Ar promoted coarsening/sintering of isolated small por-

tions of the CGO layer that is in agreement with the lower surface area of the powder heat treated in the same conditions. In spite of that, a rather porous structure was retained in the catalytic layer because of the added pore former (cellulose). The active layer has a broad distribution of pore sizes with some pores showing >1 μm diameter, probably related to the burnout of the pore former. Higher magnification images (Fig. 3c), evidenced a finer porosity in the deposited layer and CGO particles with size in the sub-micron range, both roughly estimated ~50 nm, in agreement with TEM images. Thus, SEM analyses indicate that an adequate microstructure of the catalytic layer was achieved for a durable and efficient conversion of ethanol.

After anode reduction protocol, anode-supported single cells were initially operated in (dry) hydrogen to evaluate possible effects due to the additional porous catalytic layer and to ensure water formation necessary for subsequent steam reforming of ethanol. After anode reduction and temperature stabilization, an optimal fuel (H_2) flow rate was defined by the fuel utilization $U_f = 37\%$ [35]. Such U_f was previously observed to sustain stable steam reforming of ethanol and it is close to the minimum stoichiometry when both the steam reforming and electrochemical oxidation of H_2 reactions are considered [22]. Under H_2, the performance was found to be comparable to the one of similar single cells produced and tested at FZJ indicating that the catalytic layer has no significant effect on the single cell performance [33]. Thus, fuel cell test proceeded to check stability under ethanol.

A first test included electrochemical characterizations to evaluate the stability of the direct ethanol fuel cell. The fuel cell ran continuously for 100 h with dry ethanol at 0.7 V with good stability, as shown in the inset of Fig. 4. As the internal ethanol reforming requires the water produced by the electrochemical oxidation of hydrogen, both *i* - V and impedance curves were measured under hydrogen before and after the ethanol stability test, as shown in Fig. 4.

The *i* -V curves taken before and after the ethanol durability test (Fig. 4a) are comparable. In both measurements, the OCV is close to theoretical value for dry hydrogen. The impedance diagrams of Fig. 4b show two main components: a semicircle at high frequencies and a spike at lower frequencies. Similar impedance diagrams were previously measured in electrolyte-supported SOFC using a catalytic layer [31], but the origin of the low frequency component remains to be further investigated. More important, is that data of Fig. 4 demonstrate the fuel cell operating with good stability without significant degradation. In Fig. 4b a slight increase of the ohmic resistance, possibly related to an electrical contact degradation, along with a small variation of the low frequency portion of the impedance diagram were observed after 100 h. Such features are in agreement with the small variation observed in the intermediate current range of polarization curves (Fig. 4a). The electrochemical characterization showed no significant degradation of the fuel cell during the operation under ethanol. Moreover, as compared to the rapid collapse of fuel cells without catalytic layer (Fig. 2), no loss of performance could be related to carbon deposit formation during 100 h operation in dry ethanol.

Based on the preliminary results of Fig. 4, a long term durability test on ethanol was prepared to confirm the stability towards carbon formation. In this case, a slightly higher current density was drawn from the fuel cell at 0.6 V to ensure a higher U_f to sustain both the electrochemical and catalytic reactions. Fig. 5 shows the potentiostatic long-term testing of the direct ethanol SOFC at 0.6 V.

The power density (~420 mW cm^{-2}) was fixed to values similar to the highest ones reported for direct ethanol SOFC [18]. The durability test of the fuel cell was started with H_2/N_2 (60/40%) with a flow rate of 8 L h^{-1}[35]. After 5 h of operation, the fuel was gradually changed to ethanol (see inset of Fig. 5), causing some fluctuation of the measured current values. No significant decrease of the current density occurs when changing hydrogen (~0.70 Acm^{-2}) to ethanol (~0.67 Acm^{-2}). This relatively small difference of current density in both fuels indicates that the model depicted in Fig. 1 reasonably describes the reactions taking place in the fuel cell. However, such model may not fully represent all possible reaction paths for the fuel. A relevant point is that ethanol decomposes at the operating temperature (850 °C); nevertheless, decomposition products are likely to result in coke formation if inadequate catalysts are used. Even though water is the main product of ethanol decomposition, [37] dry ethanol cannot be fed to the conventional Ni-YSZ cermet anode without severe degradation after few hours of operation, as demonstrated in Fig. 2. A possible issue is the reactivity of coke precursors, such as ethylene, which are inhibited when using Ir-CGO catalyst [22]. Thus, the results in Fig. 5 suggest

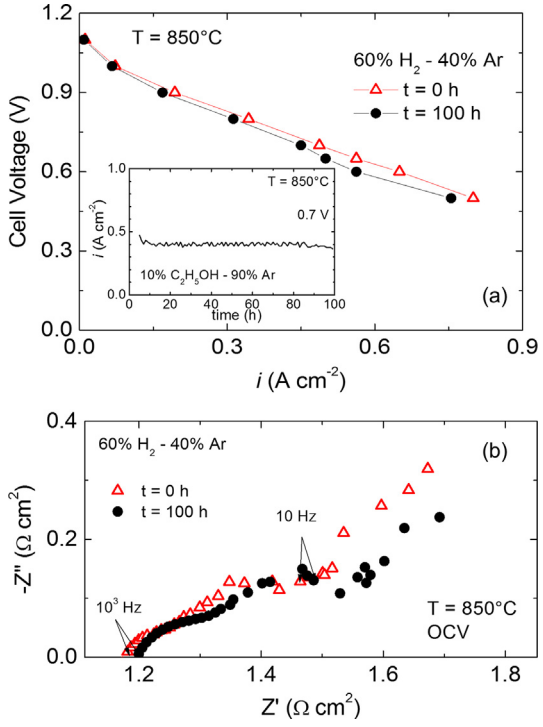

Fig. 4. (a) *i* -V curve measured under H_2 before and after the ethanol durability test. The time dependence of the current density at 0.7 V is shown in the inset. (b) Impedance diagrams (OCV) before and after 100 h of durability test on ethanol.

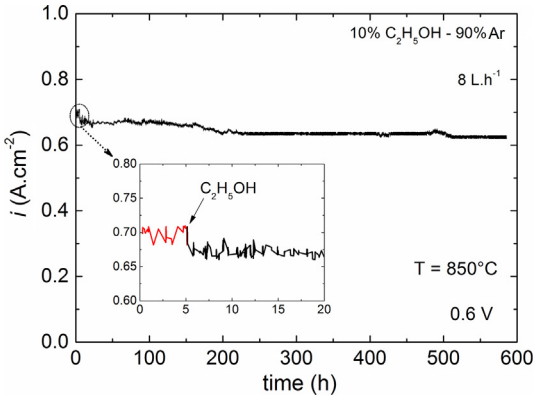

Fig. 5. Durability test at 0.6 V of the SOFC containing Ir-CGO catalytic layer under dry ethanol. The inset shows the initial hours of the test when hydrogen was changed to ethanol (t ~ 5 h).

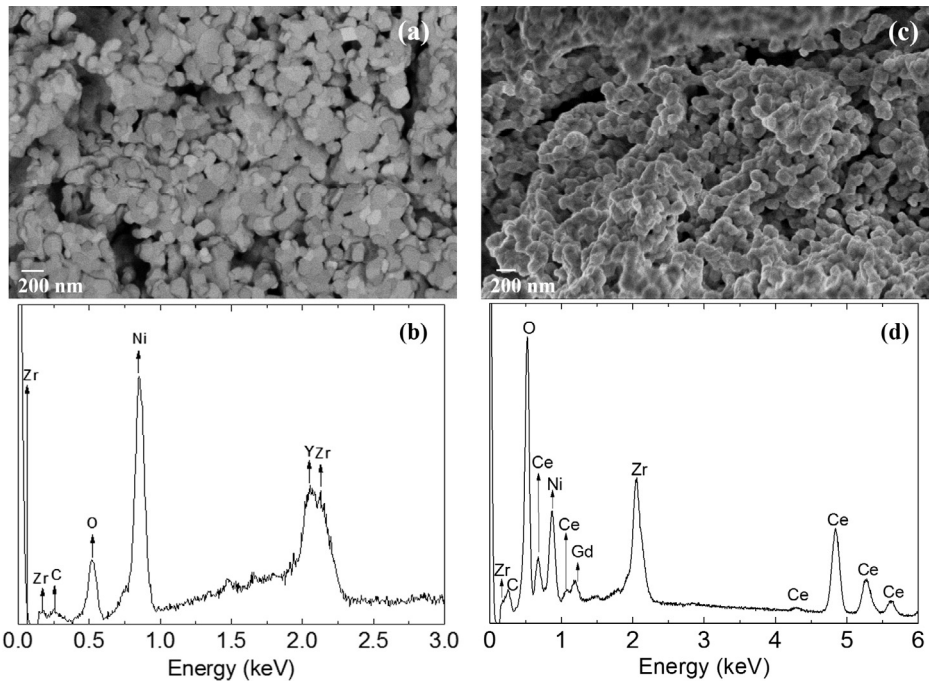

Fig. 6. Post-test analyses after 600 h operating on dry ethanol: scanning electron micrographs of (a) anode and (c) catalytic layer and the corresponding EDS analysis (b) anode and (d) anode/catalytic layer interface.

that the Ir-CGO layer is an effective catalyst for the internal reforming of ethanol. Moreover, it is a first evidence that ethanol is completely reformed resulting in 6 mol of H_2 (for 1 mol of fuel) [22].

The most important result of Fig. 5 is the stable operation of the fuel cell for ~600 h using dry ethanol. The initial 100 h of operation on ethanol showed a current output with somewhat scattered values close to the initial ~0.67 Acm^{-2}. After ~200 h the performance was slightly decreased to ~0.64 Acm^{-2} and the fuel cell reached a very stable regime up to ~500 h when the current output exhibited a decay to ~0.63 Acm^{-2} and remained very stable during the final 100 h of testing. The observed performance degradation can be associated with either electrochemical or microstructural evolution of the single cell. Similar degradation effects were previously observed in the first ~500 h of long-term SOFC testing, using similar fuel cell configuration fabricated at FZJ, and were attributed to a microstructural evolution of LSM at the cathode/electrolyte interface [44].

The excellent stability indicates that ethanol and its decomposition products have been converted in the catalytic layer without carbon deposition. It is important to consider that ethanol chemistry at the SOFC operating conditions is complex and a considerable fraction of the alcohol is pyrolysed upstream the anode. Nonetheless, the Ir-CGO layer is designed to efficiently convert the products of ethanol decomposition with no formation of graphitic carbon [22,29,34]. Such carbon species are stable and can accumulate under the studied operating conditions resulting in the collapse of the fuel cell [22,29,34]. Differently from the severe degradation of standard single cells (Fig. 2), fuel cell tests using the catalytic layer (Figs. 4 and 5) confirmed that undesirable byproducts that inhibit H_2 production and promote carbon formation (such as acetaldehyde and ethylene produced by ethanol dehydrogenation and dehydration reactions) were not formed [22]. Therefore, the experimental results confirmed that adding a catalytic layer was efficient for the direct operation of high-performance anode-supported fuel cells with (dry) ethanol.

After durability tests under ethanol, the cell was interrupted and cooled down in inert atmosphere to investigate possible carbon formation. The microstructure of both anode and catalytic layer showed no apparent evolution concerning average grain and pore sizes distributions as observed in SEM images of Fig. 6a and c, respectively. Moreover, no carbon deposits were identified in both anode layers. This observation was confirmed by EDS analysis (Fig. 6b and d). The small sign related to carbon is associated with formation of non-graphitic deposits, which can be easily oxidized and represent no major harm to fuel cell performance [14,22,32]. Such result was further confirmed by carbon content measurements that revealed a total amount of 0.014(2) wt.% of carbon in the single cell after testing. Such carbon amount is comparable to the carbon content of samples measured before the durability tests, possibly from residual additives of inks. Therefore, the small performance degradation observed after 600 h of operation in direct ethanol (Fig. 5) cannot be attributed to carbon deposit formation, which was demonstrated to be much faster and catastrophic in Fig. 2. Thus, the catalytic layer played a major role on the conversion of ethanol and its pyrolysis byproducts, inhibiting the formation of carbon-precursor compounds and providing hydrogen for the electrochemical reaction at the Ni-anode. Both the absence of carbon combined with the small variation in the current density during the durability tests are strong indications that the steam reforming reaction (Eq. (1)) is almost stoichiometric using water produced in the anode. Further experiments are underway to analyze both the gas outlet and investigate the impedance diagrams of cells with a catalytic layers running on ethanol.

4. Conclusions

High-performance solid oxide fuel cells accumulated ~700 h of operation with dry ethanol without degradation due to carbon formation. A highly active catalyst with nanosized particles of Ir-CGO was efficient to promote the ethanol steam reforming using the water generated by the electrochemical conversion of hydrogen at the anode/electrolyte interface. The catalytic layer promotes overall steam reforming reactions of ethanol that result in similar current outputs in both hydrogen and ethanol fuels. The current

output was similar to the highest reported values for direct ethanol SOFCs. The harsh conditions used for the durability test, i.e., no water added, indicate that the studied fuel cell configuration is a promising device for using an available and efficient renewable biofuel such as bioethanol. The experimental results confirm that the bilayer anode is viable in high-performance anode-supported cells. Moreover, the results point to the dissemination of carbon-neutral SOFCs.

Acknowledgments

Thanks are due to Brazilian agencies FAPESP (2013/26961-7; 2014/50767-9; 2014/09087-4; 2014/50279-4) and CNEN. FCF is a CNPq fellow (306258/2016-1). Authors thank Ms. Lühring of the Central Institute for Engineering, Electronics and Analytics (ZEA-3) of FZJ for the carbon content measurements and for M. Aouine (IRCELyon, France) for TEM images.

References

[1] Frölicher TL. Strong warming at high emissions. Nat Climate Change 2016;6:823–4.
[2] Singhal SC, Kendall K, High temperature and solid oxide fuel cells – fundamentals, (2003) Design and Applications, p. 1, Ed. Elsevier.
[3] Minh NQ. Ceramic fuel cells. J Am Ceram Soc 1993;76:563–88.
[4] Atkinson A, Barnett S, Gorte RJ, Irvine JTS, McEvoy AJ, Mogensen M, et al. Advanced anodes for high-temperature fuel cells. Nat Mat 2004;3:17–27.
[5] Wachsman ED, Marlowe CA, Lee KT. Role of solid oxide fuel cells in a balanced energy strategy. Energ Environ Sci 2012;5:5498–509.
[6] Qu J, Wang W, Chen Y, Deng X, Shao Z. Stable direct-methane solid oxide fuel cells with calcium-oxide-modified nickel-based anodes operating at reduced temperatures. Appl Energ 2016;164:563–71.
[7] Lin Y, Zhan Z, Liu J, Barnett SA. Direct operation of solid oxide fuel cells with methane fuel. Solid State Ionics 2005;176:1827–35.
[8] Kaur G, Basu S. Performance studies of copper-iron/ceria-yttria stabilized zirconia anode for electro-oxidation of methane in solid oxide fuel cells. Int J Energy Res 2015;39:1345–54.
[9] Gorte RJ, Park S, Vohs JM, Wang C. Anodes for direct oxidation of dry hydrocarbons in a solid-oxide fuel cell. Adv Mater 2000;12:1465–9.
[10] McIntosh S, Gorte RJ. Direct hydrocarbon solid oxide fuel cells. Chem Rev 2004;104:4845–65.
[11] Kaur G, Basu S. Study of carbon deposition behavior on Cu-Co/CeO2-YSZ anodes for direct butane solid oxide fuel cells. Fuel cells 2014;14:1006–13.
[12] Zhan Z, Barnett SA. An octane-fueled solid oxide fuel cell. Science 2005;308:844–7.
[13] Zhan Z, Barnett SA. Use of a catalyst layer for propane partial oxidation in solid oxide fuel cells. Solid State Ionics 2005;176:871–9.
[14] Deluga GA, Salge JR, Verykios XE. Renewable hydrogen from ethanol by autothermal reforming. Science 2004;303:993–7.
[15] Badwal SPS, Giddey S, Kulkarni A, Goel J, Basu S. Direct ethanol fuel cells for transport and stationary applications – a comprehensive review. Appl Energ 2015;145:80–103.
[16] Gomes RS, De Bortoli AL. A three-dimensional mathematical model for the anode of a direct ethanol fuel cell. Appl Energ 2016;183:1292–301.
[17] Huang B, Zhu X, Hu W, Wang Y, Yu Q. Characterization of the Ni-ScSZ anode with a LSCM–CeO_2 catalyst layer in thin film solid oxide fuel cell running on ethanol fuel. J Power Sources 2010;195:3053–9.
[18] Armstrong EN, Park J, Minh NQ. High-performance direct ethanol solid oxide fuel cells. Electrochem Solid-State Lett 2012;15:B75–7.
[19] Lo Faro M, Reis RM, Saglietti GGA, Zignani SC, Trocino S, Frontera P, et al. Investigation of Ni-based alloy/CGO electrocatalysts as protective layer for a solid oxide fuel cell fed with ethanol. J Appl Electrochem 2015;45:647–56.
[20] Morales M, Espiell F, Segarra M. Improvement of performance in low temperature solid oxide fuel cells operated on ethanol and air mixtures using Cu-ZnO-Al_2O_3 catalyst layer. J Power Sources 2015;293:366–72.
[21] Liao M, Wang W, Ran R, Shao Z. Development of a Ni–$Ce_{0.8}Zr_{0.2}O_2$ catalyst for solid oxide fuel cells operating on ethanol through internal reforming. J Power Sources 2011;196:6177–85.
[22] Nobrega SD, Gélin P, Georges S, Steil MC, Augusto BL, Noronha FB, et al. A fuel-flexible solid oxide fuel cell operating in gradual internal reforming. J Electrochem Soc 2014;161:F354–9.
[23] Muccillo R, Muccillo ENS, Fonseca FC, de Florio DZ. Characteristics and performance of electrolyte-supported solid oxide fuel cells under ethanol and hydrogen. J. Electrochem Soc 2008;155:B232–5.
[24] Ni M, Leung DYC, Leung MKH. A review on reforming bio-ethanol for hydrogen production. Int J Hydrogen Energ 2007;32:3238–47.
[25] Nissan Motor Corporation, Nissan announces development of the world's first SOFC-powered vehicle system that runs on bioethanol electric power, <https://newsroom.nissan-global.com/releases/160614-01-e, 2016 (press release on June 14th>).
[26] Aslannejad H, Barelli L, Babaie A, Bozorgmehri S. Effect of air addition to methane on performance stability and coking over NiO–YSZ anodes of SOFC. Appl Energ 2016;177:179–86.
[27] Sivaprakash S, Choi S, Jun A, Shin TH, Ju Y-W, Jeong HY, et al. Layered oxygen-deficient double perovskite as an efficient and stable anode for direct hydrocarbon solid oxide fuel cells. Nat Mater 2015;14:205–9.
[28] Vernoux P, Guindet J, Kleitz M. Gradual internal methane reforming in intermediate-temperature solid oxide fuel cells. J Electrochem Soc 1998;145:3487–92.
[29] Klein JM, Hénault M, Gélin P, Bultel Y, Georges S. A solid oxide fuel cell operating in gradual internal reforming conditions under pure dry methane. Electrochem Solid-State Lett 2008;11:B144–7.
[30] Klein JM, Hénault M, Roux C, Bultel Y, Georges S. Direct methane solid oxide fuel cell working by gradual internal steam reforming: analysis of operation. J Power Sources 2009;193:331–7.
[31] Nobrega SD, Galesco MV, Girona K, de Florio DZ, Steil MC, Georges S, et al. Direct ethanol solid oxide fuel cell operating in gradual internal reforming. J Power Sources 2012;213:156–9.
[32] Augusto BL, Noronha FB, Fonseca FC, Tabuti FN, Colman RC, Matos LV. Nickel/gadolinium-doped ceria anode for direct ethanol solid oxide fuel cell. Int J Hydrogen Energ 2014;39:11196–209.
[33] Tietz F, Fu Q, Haanappel VAC, Mai A, Menzler NH, Uhlenbruck S. Int J Appl Ceram Technol 2007;4:436;
Fonseca FC, Uhlenbruck S, Nédélec R, Buchkremer HP. J. Power Sources 2010;195:1599.
[34] Wisniewski M, Boréave A, Gélin P. Catalytic CO2 reforming of methane over Ir/$Ce_{0.9}Gd_{0.1}O_{2-x}$. Catal Commun 2005;6:596–600.
[35] Nobrega SD, Steil MC, Georges S, Uhlenbruck S, Fonseca FC. Direct ethanol anode-supported solid oxide fuel cell. J Electrochem Soc Trans 2015;68:2851–8.
[36] Ferlauto AS, de Florio DZ, Fonseca FC, Esposito V, Muccillo R, Traversa E, Ladeira LO. Chemical vapor deposition of multi-walled carbon nanotubes from nickel/yttria-stabilized zirconia catalysts. Appl Phys A 2006;84:271–6.
[37] Mattos LV, Jacobs G, Davis BH, Noronha FB. Production of hydrogen from ethanol: review of reaction mechanism and catalyst deactivation. Chem Rev 2012;112:4094–123.
[38] Gupta GK, Dean AM, Ahn K, Gorte RJ. Comparison of conversion and deposit formation of ethanol and butane under SOFC conditions. J Power Sources 2006;158:497–503.
[39] da Costa LOO, da Silva AM, Noronha FB, Mattos LV. The study of the performance of Ni supported on gadolinium doped ceria SOFC anode on the steam reforming of ethanol. Int J Hydrogen Energ 2012;37:5930–9.
[40] Toyir J, Gélin P, Belatel H, Kaddouri A. Ir/$Ce_{0.9}Gd_{0.1}O_{2-x}$ as a new potential anode component in solid oxide fuel cells integrating the concept of gradual internal reforming of methane. Catal Today 2010;157:451–5.
[41] Cheah SK, Massin L, Aouine M, Steil MC, Fouletier J, Gélin P, Mechanism of methane steam reforming on Ir supported on gadolinium doped ceria catalyst in water deficient conditions (2017) submitted to J. Catal. B.
[42] Tsoga A, Naoumidis A, Stöver D. Total electrical conductivity and defect structure of ZrO_2-CeO_2-Y_2O_3-Gd_2O_3 solid solutions. Solid State Ionics 2000;135:403–9.
[43] Esposito V, Ni DW, Marani D, Teocoli F, Thydén KTS, de Flório DZ, et al. Accelerated ceria–zirconia solubilization by cationic diffusion inversion at low oxygen activity. J Mater Chem A 2016;4:16871–8.
[44] de Haart LGJ, Mougin J, Posdziech O, Kiviaho J, Menzler NH. Stack degradation in dependence of operation parameters; the real-SOFC sensitivity analysis. Fuel Cells 2009;9:794–804.